ELSEVIER

Mechanics of Materials 34 (2002) 627–642

MECHANICS OF MATERIALS

www.elsevier.com/locate/mechmat

Large strain constitutive behavior of OFHC copper over a wide range of strain rates using the shear compression specimen

D. Rittel [*,1], G. Ravichandran, S. Lee

Graduate Aeronautical Laboratories, Mail Stop 105-50, California Institute of Technology, Pasadena, CA 91125, USA

Received 2 February 2002; received in revised form 15 April 2002

Abstract

A new specimen geometry, the shear compression specimen (SCS), has been developed and validated for large strain testing of metals over a wide range of strain rates. A detailed numerical analysis of this specimen is presented to assess its range of applications and limitations. The dominant deformation mode of the gage section of the SCS is found to be shear. The stress and strain state in the gage section is necessarily three-dimensional, in contrast with commonly assumed situations of simple shear. Yet, considerable simplification is gained through the introduction of simple approximations for the Mises equivalent stress and plastic strain. These fields are found to be uniformly distributed over the gage section. The SCS framework is applied to the characterization of the large strain behavior of OFHC copper over a range of strain rates $\dot{\varepsilon}_e = 10^{-3}$ to 3.2×10^4 s^{-1}. The strain rate sensitivity of the material is noted, in accord with previous observations. The mechanical tests are complemented by microstructural characterization of the material which corroborate the numerical predictions of uniformity of the equivalent strain. The grains in the gage section are discernable for true strains less than 2. At larger strains, of the order of 3.5, the individual grains are no longer discernable and small equiaxed grains are observed, using scanning electron microscopy. These grains are characteristic of recrystallized material. The use of a single specimen geometry coupled to simple data reduction procedures is expected to promote constitutive characterization at large strains over a seamless range of strain rates.

Keywords: Shear compression specimen; Constitutive; Large strain; Strain rate; OFHC copper; Recrystallization

1. Introduction

Large plastic strains accumulate in metals during manufacturing processes such as rolling, forming and (high-speed) machining, and as well as in ballistic failure, dynamic crack growth and shear banding (Meyers, 1994). Accurate modeling of these processes requires that the material behavior be determined at large strains over a wide

* Corresponding author. Tel.: +1-972-4-8293261; fax: +1-972-4-834533.

E-mail addresses: merittel@tx.technion.ac.il (D. Rittel), ravi@aero.caltech.edu (G. Ravichandran).

[1] Faculty of Mechanical Engineering, Technion, Haifa, Israel.

0167-6636/02/$ - see front matter
PII: S0167-6636(02)00164-3

range of temperatures and strain rates (e.g. Clifton, 1990; Bodner and Rubin, 1994). The attainment of large strains, using uniaxial testing, is often limited by the development of plastic instabilities (necking, barreling). This situation can be improved by torsion testing of thin tubes. Unfortunately, specimen shakedown or failure is likely to occur at a premature stage of the test. As an alternative, shear testing is often used with the complication related to the fact that a state of pure (or even simple) shear is not easily achieved in most specimen geometries. When a ductile material is tested in shear, large strains develop over a narrow gage section, whose width is not accurately known. Therefore, little is known about the nature and the uniformity of the mechanical fields.

The dynamic nature of many of the abovementioned processes has motivated the study of high-strain-rate deformations. Thin-walled torsion specimens have been used in a Kolsky (split Hopkinson) torsion bar apparatus (e.g. Duffy et al., 1971) for studying high-strain-rate behavior of metals in shear. To achieve large shear strains, specimen geometries were devised in which the linear displacement applied at the specimen boundary was translated into local shear in the gage section. An example of such a specimen is the so-called "top hat specimen" which was developed by Meyer and Manwaring (1986), and used thereafter by many other researchers. Another variant is the double shear specimen used by Klepaczko (1998) to study high-strain-rate shear deformation. Finally, at very high strain rates, a simple specimen geometry (thin disc) has been used by Clifton and Klopp (1986) in their pressure-shear plate impact experiments. In all these tests, emphasis was on the shear nature of the deformation.

While stress/strain uniformity in the specimen or the gage section must be assessed by numerical techniques, uniformity is generally assumed so that simple relations can be used to determine the shear strain and stress, e.g. Minnaar and Zhou's (1998) comparative study of the shear response of various alloys. Finally, when a large range of strain rates is to be explored, different specimens are generally used, adding to the complexity of the determination of the constitutive behavior at large strains. Typically two gaps exist in the constitutive data for strain rates of interest, between 10^0–10^2 and 10^4–10^5 s^{-1}. Due to various limitations in the testing techniques as well as the specimen geometry, data in these regimes of strain rates is rather sparse. From this brief review, it appears that there is a need for a single specimen for large strains experiments, over a wide range of strain rates (and temperatures), and for which data reduction remains as simple as possible. This paper reports our results regarding the development and application of such a specimen to the constitutive characterization of OFHC copper over a wide range of strain rates and large strains.

The paper is organized in the following four main sections: first, we address the issue of specimen design, characterization and validation through detailed numerical simulations using the finite element method. Next, based on the numerical study, simplified relations between the specimen geometry, loads, prescribed displacements and the stresses and strains are presented. The second section is concerned with the experimental aspects, and it addresses the mechanical behavior of OFHC copper. The specimen is validated experimentally by performing cross-comparisons with other well-established specimen geometries and previous results on this material. The third section concerns the material behavior itself. The stress–strain behavior is characterized over strain rates ranging from 10^{-3} to 3.5×10^4 s^{-1}. The rate sensitivity of the flow stress is evaluated and the results from microstructural characterization are reported. These results do not only characterize the material but also the uniformity of the deformation in the gage. The last section consists of a brief discussion and concluding remarks for the study.

2. Specimen design and validation

2.1. The shear compression specimen

The shear compression specimen (SCS) is schematically depicted in Fig. 1. The SCS consists of a short cylinder into which two slots have been machined at 45° to the longitudinal axis. Upon

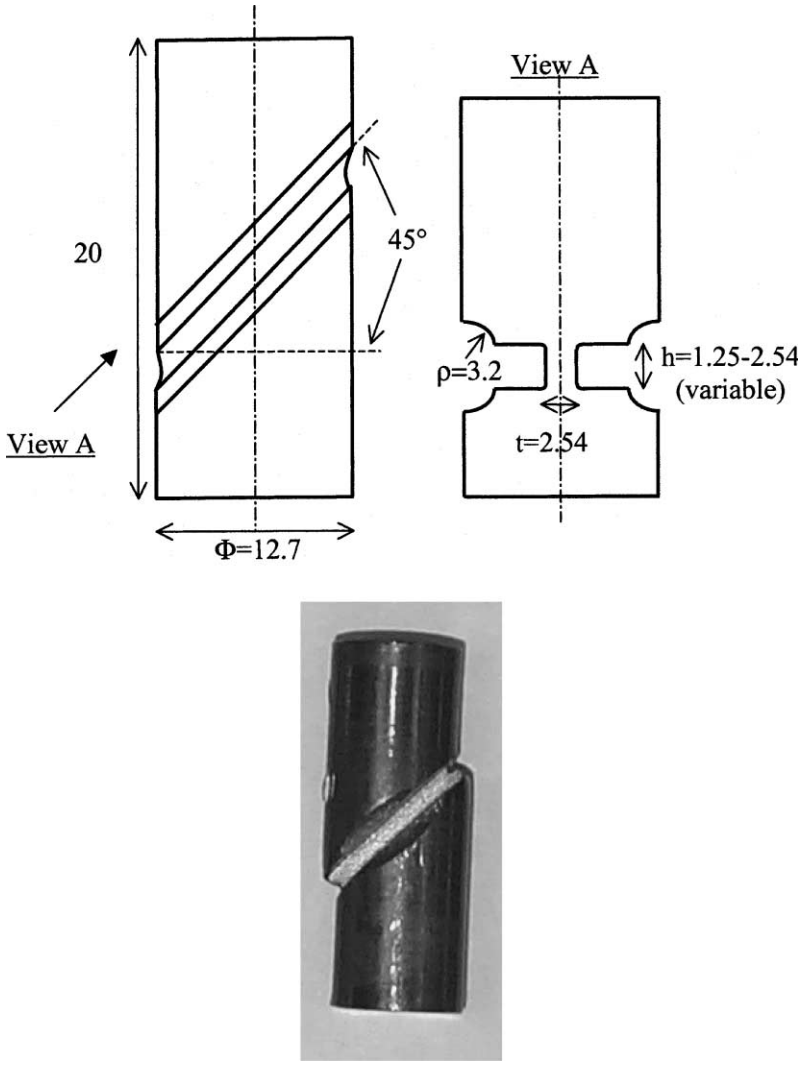

Fig. 1. Schematic representation of the SCS. All dimensions are in mm. h, t and Φ are the geometrical parameters used for stress and strain determination. The deformed specimen is made of commercial copper.

compression of the cylinder, the gage section experiences a dominant state of shear deformation. The gage section is defined by its height (h) and thickness (t). The diameter of the cylindrical sections (Φ) is chosen such that they remain elastic during the test. These sections transfer the vertical displacements and loads to the gage. A clearance (ρ) is machined, to provide visual access to the gage and facilitate diagnostics (e.g. real-time temperature monitoring, or deformation related features). The clearance does not affect load transmission to the gage. A typical deformed copper specimen is also shown in Fig. 1. In this figure the shear dominated nature of the gage deformation is clearly illustrated.

2.2. Numerical analysis of the shear compression specimen

2.2.1. Finite element model and results

The SCS was discretized for three-dimensional, implicit, static finite element analysis, using eight

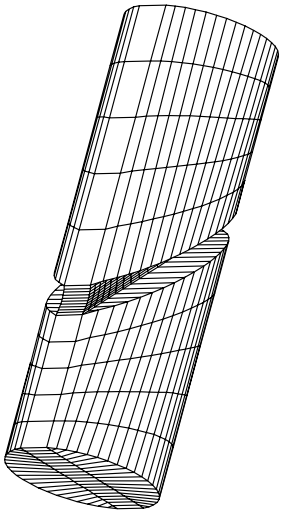

Fig. 2. The meshed specimen used for finite element calculations.

node isoparametric brick-type elements (Fig. 2). The model comprised about 800 elements and was solved using the *ABAQUS* finite element code (Hibbitt et al., 1996). Uniform vertical displacements (d) were applied to the upper boundary of the specimen, while the motion of the lower boundary (base) was constrained in the vertical direction only (no lateral frictional constraint) (Fig. 3). The analysis accounts for large deformations (geometrical non-linearities) and large strains. The material behavior was modeled by a bilinear (elastic and linear hardening) isotropic hardening J_2 plasticity. Two generic material behaviors were considered, having identical Young's modulus and yield stress, but having different hardening moduli (Table 1). These materials were selected to represent a typically "soft" and a typically "hard" material, to represent two extreme types of material response. In the sequel, the calculated stresses and strains are referred to the deformed configuration and are therefore true stresses and true strains. Stresses and strains are expressed in the local gage coordinate system (denoted by subscript b in Fig. 3).

2.2.2. Boundary conditions for the gage section

The first result concerns the influence of the stiffness of the cylindrical sections of the SCS on

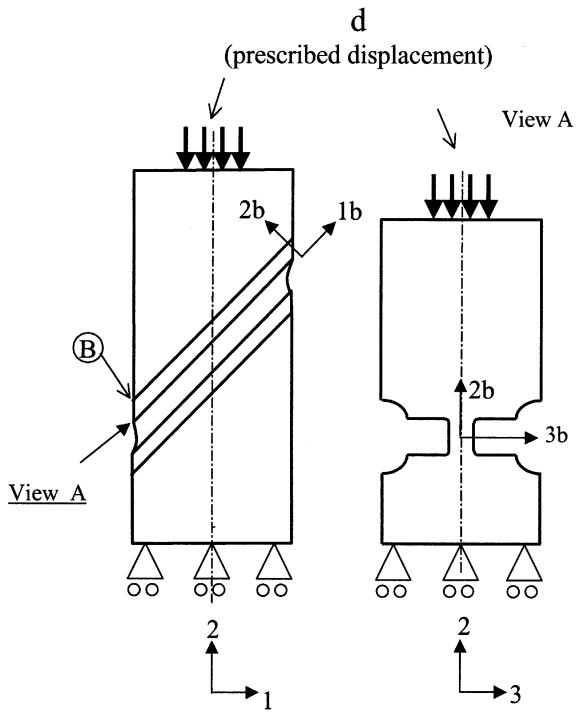

Fig. 3. Schematic representation of the boundary conditions for the numerical model. The local gage coordinate system is indicated by subscript b. B indicates the control point for which vertical displacements were calculated as a function of the prescribed displacement d, as shown in Fig. 4.

Table 1
Constitutive parameters for the two types of model metals

Material	Yield stress (MPa)	Young's modulus (GPa)	Poisson's ratio	Hardening modulus
Hard	400	210	0.33	E/100
Soft	400	210	0.33	E/500

the displacements exerted on the gage section. A verification of the vertical displacement of two symmetrically located edge points on the gage showed that the two points experience identical vertical displacements, regardless of the kind of material, as shown for one point (B) in Fig. 4. For the hard material, the local displacement is identical to the prescribed displacement for a limited range only (up to $d = 0.7$ mm, $d/h = 0.28$). By contrast, the local and prescribed displacements

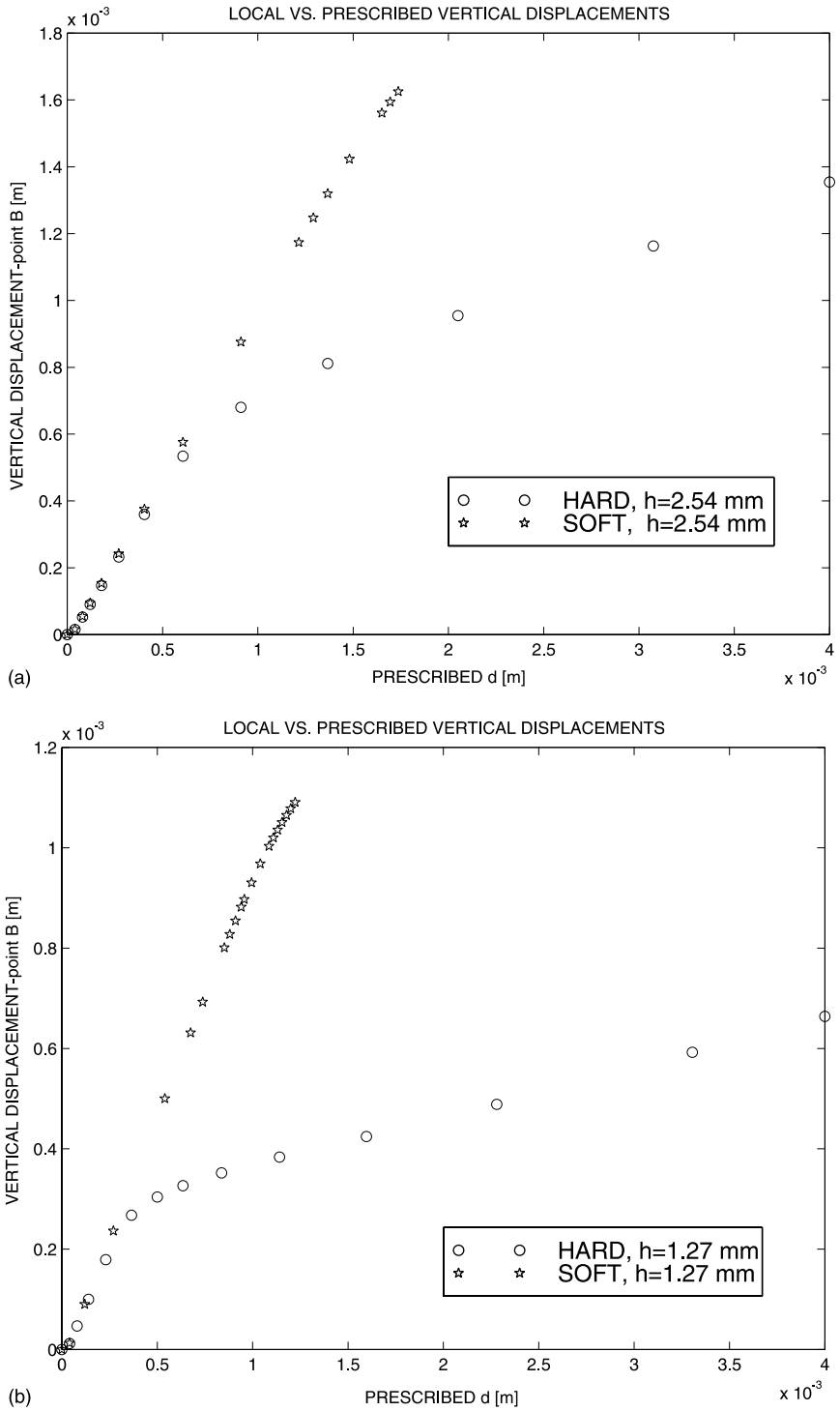

Fig. 4. Computed vertical displacements of the representative gage point B, as a function prescribed *d*. Note that for the soft material, there is a one to one correlation between these two displacements, (a) 2.54 mm gage height, (b) 1.27 mm gage height.

are virtually identical for the soft material for the overall prescribed displacement range. As shown in Fig. 4, reduction of the gage height (h) to half its previous value yielded similar results. The relation between local and prescribed displacements remains as before, with the distinction that the matching range for the hard specimen is now reduced to about half its previous value, i.e. about 0.35 mm. These results show that the cylindrical parts of the SCS just transfer the load to the gage section without any undue permanent deformation. In this aspect, the cylindrical parts of the SCS remain elastic similar to the discs confining the specimen in the pressure-shear configuration (Clifton and Klopp, 1986). It is therefore concluded that the boundary displacements are identical to those experienced by the gage section for a soft material, regardless of the gage height.

2.2.3. Stress and strain fields

The shear strain and shear stress distributions, expressed the local gage system, are shown in Fig. 5a and b respectively for a prescribed boundary displacement of $d = 1$ mm. While these results characterize the soft material, similar results were obtained for the hard material, indicating that the shear stress and strain fields are reasonably uniform in the gage of the SCS. The equivalent plastic strain and (Mises) stress is shown for the same specimen, in Fig. 6a and b, respectively. A localized stress concentration is noticeable along the transition region from the cylindrical part to the gage section. This transition region was modeled as a right angle, whereas in reality, this sharp corner becomes a fillet during the machining process. These figures confirm the uniformity of the equivalent stress and strain fields in the vast majority of the gage section.

Additional insight is gained by considering the individual stress (strain) components in the gage section. The element at the center of the gage section was selected, as representative on the basis of the uniformity of the stress and strain fields. Characteristic results are shown in Figs. 7 and 8. These figures show that the gage section experiences non-proportional loading in which each

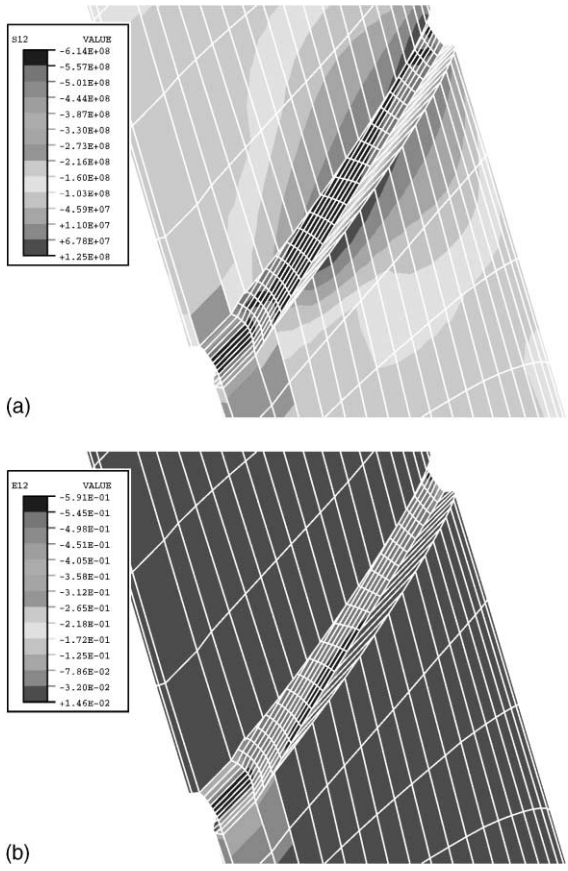

Fig. 5. Computed shear stress (a) and shear strain (b) components in the local gage coordinate system. Soft material, $h = 2.54$ mm, prescribed $d = 1$ mm.

stress component evolves independently with a noticeable confining effect of the negative stress components. Examination of the strain components indicates a dominance of the shear strain component, ε_{12}. These results also indicate that the kinematics of the deformation and the resulting stress distribution are not amenable to a simple analytical description such as simple shear, which is commonly assumed for other kinds of shear specimen geometries.

It can thus be concluded that the stress and strain fields are reasonably uniform in the gage section. While the stress and strain components do not correspond to simple shear, the gage deformation is dominated by shear.

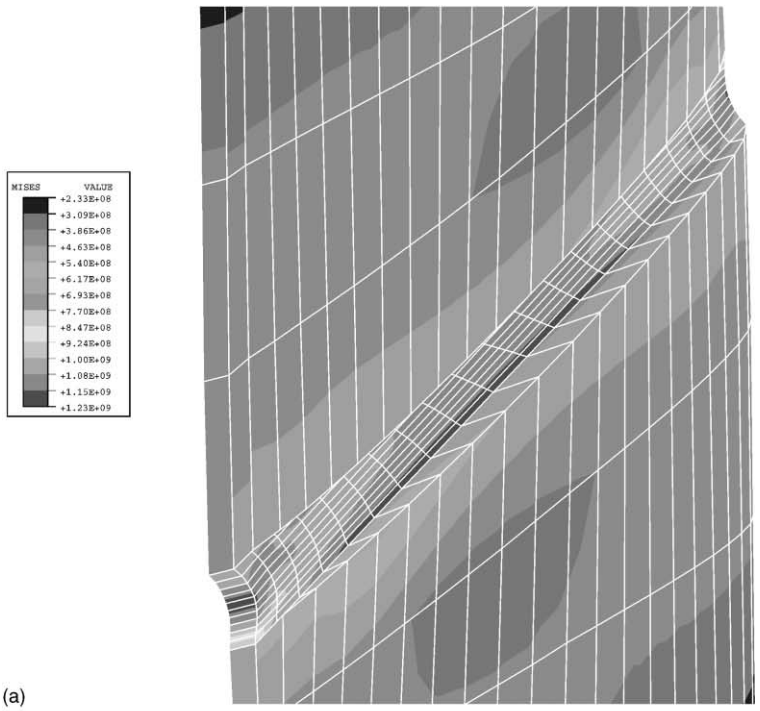

Fig. 6. Computed Mises equivalent stress (a) and equivalent plastic strain (b), expressed in the local gage coordinate system. Soft material, $h = 2.54$ mm, prescribed $d = 1$ mm.

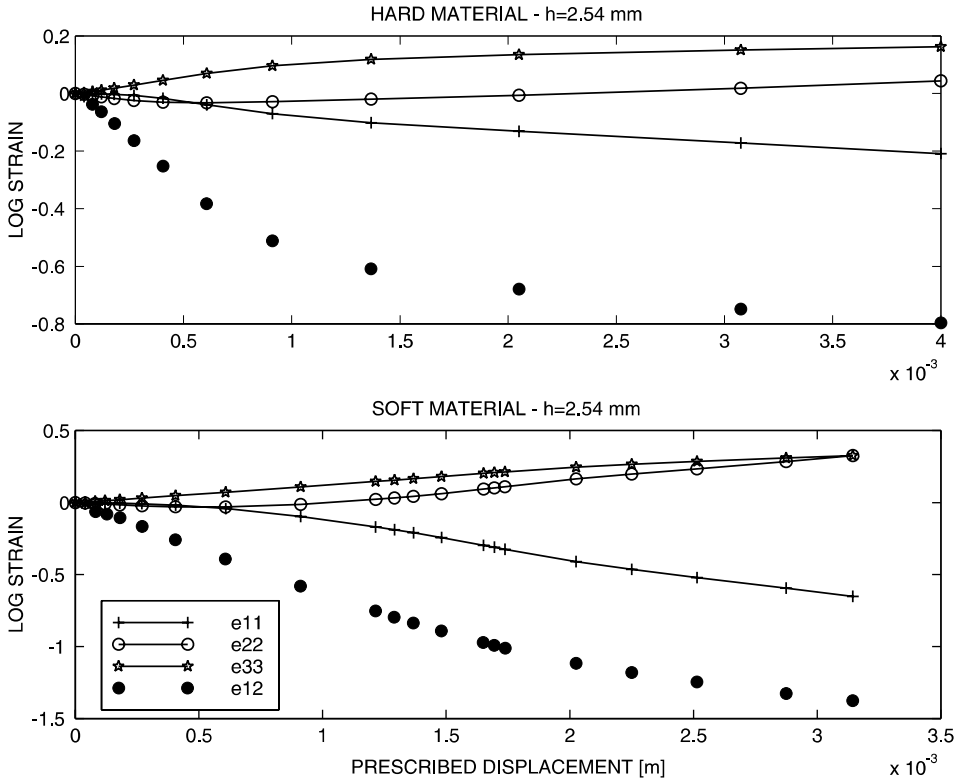

Fig. 7. Calculated strain components in an element located in the center of the gage, at mid-thickness.

2.2.4. Kinematics of deformation and stress state

Based on the specimen geometry and loading (Fig. 2a), a material element in the gage section of the deforming SCS specimen can be idealized as shown in Fig. 9. h is the height of the gage section and ψ is the angle between the normal to the gage section and the axis of loading. Φ and t are the diameter of the cylindrical section and thickness of the gage section respectively. In the present investigation, ψ is chosen to be 45° to coincide with the plane of maximum shear. X_i and x_i are the cartesian coordinates of the position vector of a particle in the undeformed (reference) and deformed (current) configurations of axes aligned with the gage section, respectively.

Assuming the deformation to be isochoric (since no volume change occurs during plastic flow), the kinematics of deformation can be expressed as:

$$\begin{aligned} x_1 &= (1-\lambda)X_1 + \kappa X_2 \\ x_2 &= X_2/(1-\lambda^2) \\ x_3 &= (1+\lambda)X_3 \end{aligned} \tag{1}$$

where κ and λ, are the amount of shear and lateral extension in the thickness direction respectively. $\lambda = 0$ corresponds to the case of simple shear. However, due to the finite value of h, λ is not equal to zero which results in normal deformation in the X_3 and X_1 directions, and to preserve volume, in the X_2 direction also. For a prescribed normal displacement in the axial direction of the cylinder, the shear κ can be approximated from the geometry as $d\tan\psi/h$, and hence for $\psi = 45°$, $\kappa = d/h$. However, λ is far more complicated to be described by simple analytical formula since this is dependent on the assumption made regarding the state of stress or deformation in the thickness direction (X_3), e.g. plane stress.

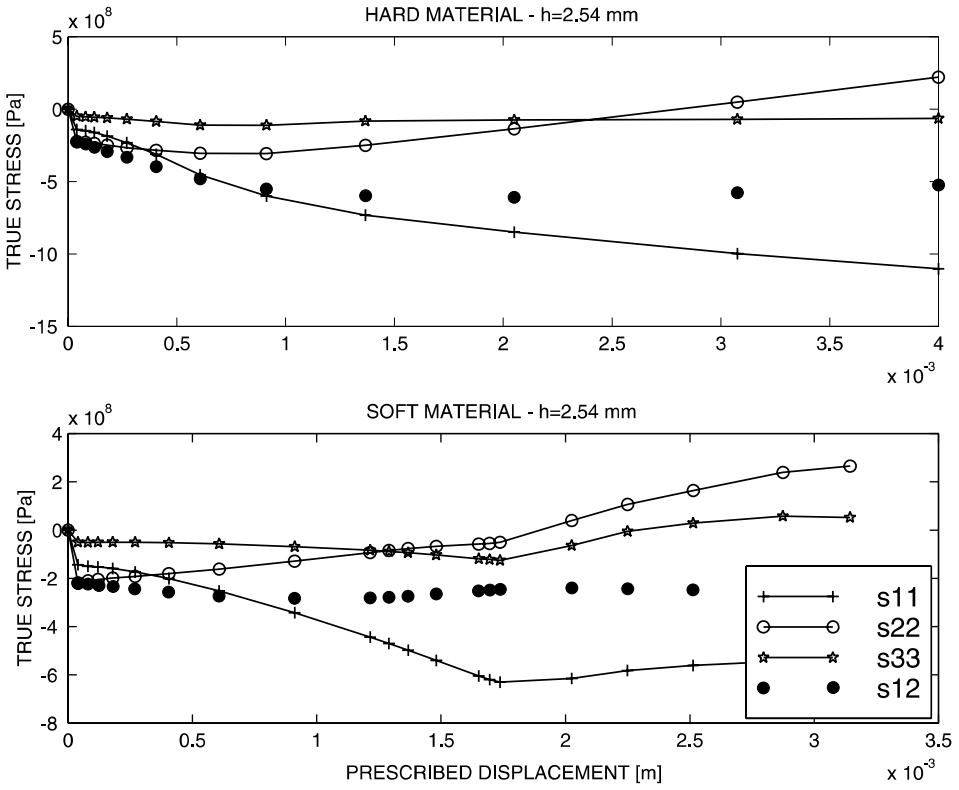

Fig. 8. Calculated stress components in an element located in the center of the gage, at mid-thickness.

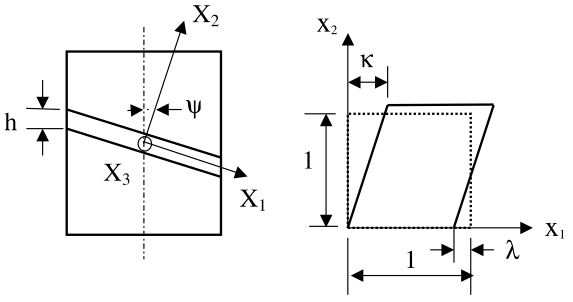

Fig. 9. Schematic representation of the specimen geometry and kinematics of deformation in the gage section.

2.2.5. A simple stress–strain relationship

The next step is the identification of a simple relationship expressing the equivalent true stress (σ_e), equivalent plastic strain (ε_e), strain rate ($\dot{\varepsilon}_e$) and applied load (P) in terms of the geometrical parameters of the SCS and the applied loads. Based on the results of the foregoing finite element analysis, the following relations are proposed:

$$\varepsilon_e = \frac{d}{h}; \quad \dot{\varepsilon}_e = \frac{\dot{d}}{h} \tag{2}$$

$$\sigma_e = 0.85(1 - 0.2\varepsilon_e)\frac{P}{\phi t} \tag{3}$$

These simple approximations hold very well, irrespective of the gage height, for equivalent strains of typically $\varepsilon_e = 0.4$ for the hard material (Rittel et al., 2000) and $\varepsilon_e = 1$ for the soft material (Fig. 10). At the present stage, these relations apply to a limited strain range. Additional specialized calculations are needed to extend their range of validity to higher strains.

Therefore, in the given strain range, measured loads and displacements can be used to determine the equivalent true stress–plastic strain relationship, as shown in the next section.

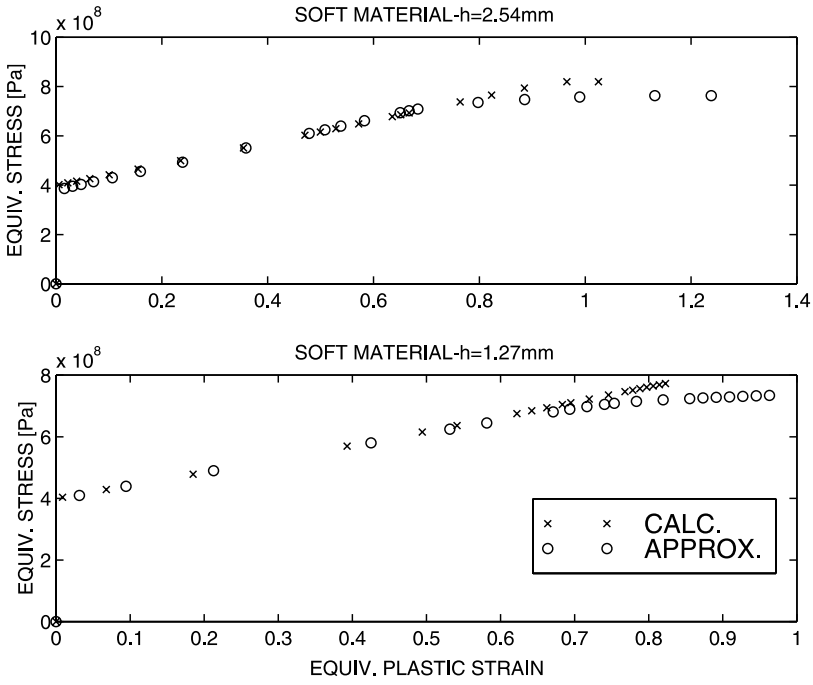

Fig. 10. Calculated and approximated (Eqs. (1) and (2)) equivalent stresses and strains. Soft material with two gage heights. The approximation is excellent up to typically $\varepsilon_{eq} = 1$.

3. Experimental results

3.1. Material and experimental

The material selected for detailed investigation using the SCS specimen geometry was OFHC (copper), obtained in the form of a 12.54 mm (Φ) diameter bar. The material was tested in this as-received condition without heat treatment of any kind. SCS specimens were machined with various nominal gage heights, h (2.54 mm, 1.27 mm, and 0.7 mm), along with cylindrical specimens (CS), 7.5 mm in diameter and of varying lengths (12.5 mm, 7.5 mm) to reach various strain rates.

Quasi-static testing was first carried out on an INSTRON screw driven machine to "calibrate" the SCS versus the CS. Additional testing was carried out on a servo-hydraulic MTS machine (displacement control) to reach higher crosshead velocities resulting in higher strain rates. High strain rate compressive testing was carried out using a Kolsky (split Hopkinson) pressure bar (Kolsky, 1949). The data reduction procedure and preliminary results can be found in Rittel et al. (2000).

3.2. A comparison between SCS and CS

As reported in Rittel et al. (2000), the flow curves obtained in the quasi static (10^{-4} and 10^{-3} s^{-1}) and dynamic (up to 9×10^3 s^{-1}) strain rate regime were quite similar for both CS and SCS specimens. This observation validates the overall SCS concept proposed here. In the sequel, we will address additional experiments performed recently at higher and intermediate strain rates.

3.3. The SCS at high strain rates

High-strain-rates experiments were carried out on SCS with a gage height of $h = 1.20$ mm. In these experiments, the nominal strain rate, according to Eq. (1) was 32,000 s^{-1}. A typical stress–strain curve is shown in Fig. 11. The data have

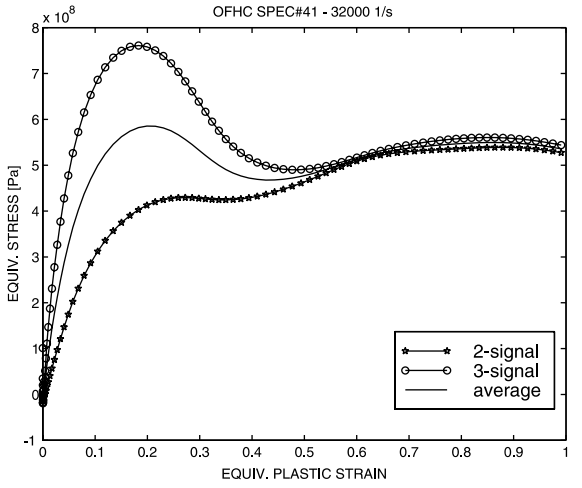

Fig. 11. Experimental stress–strain curve for an OFHC specimen deformed at a nominal strain rate of 32,000 s^{-1}. Results are plotted for the complete analysis (3-signal), assuming equilibrium (2-signal) and their average.

been processed using all three incident, reflected and transmitted signals (3-signal), and assuming 3specimen equilibrium (2-signal), Rittel et al. (2000). As shown in this figure, the two calculations yield different results up to an initial strain of 0.4. Past this initial strain where transient effects are important, the stress–strain curves become identical. The observed initial discrepancy between the two analyses stems from the fact that the length of the SCS is finite, so that a certain time is required for equilibrium to establish over the entire cylindrical *specimen as a whole*. This state of affairs is well known in relation to high strain rate testing with a Kolsky bar. However, as noted in Rittel et al. (2000), the small gage dimensions allow for *gage* (*local*) *equilibrium* to be reached at a much earlier stage of the deformation. Therefore, the equilibrium assumption (2-signal) is probably closer to the actual stress state in the gage than the strongly oscillating prediction of the full (3-signal) analysis.

Nevertheless, the conservative approach adopted here is to use the average stress–strain curve while reporting quantitative results in the range of overlap between the two approaches, that is $\varepsilon_e = 0.4$–1, in this specific case. This same approach was adopted and validated through the successful comparison of the results obtained with SCS and cylindrical specimens at a strain rate of 9000 s^{-1}.

It is worth noting that the highest strain rate reported here is 32,000 s^{-1}. Yet, this value is not a limit, as higher rates could be reached by additional shortening of the gage height. The present result shows that the strain-rate gap between 10^4 s^{-1} (Kolsky bar) and 10^5 s^{-1} (pressure-shear plate impact) can thus be bridged by means of the SCS.

3.4. The SCS at low strain rates

Quasi-static experiments are seldom carried out at rates in excess of 1 s^{-1}. Consequently, there is a gap in the 1–100 s^{-1} range of strain rates that cannot be bridged easily using conventional testing equipment or specimens. A series of tests was carried out using SCS specimens with a gage height of 0.7 mm, loaded by means of a servo-hydraulic machine. In these experiments, the highest crosshead velocity was 40 mm/s. The results presented below have been corrected with respect to the stiffness of the loading train, i.e. machine compliance. Typical strain rates achieved in this series of experiments was $\dot{\varepsilon}_e = 0.6$, 13, 38 and 59 s^{-1}. It is readily observed that these strain rates lie exactly in the above-mentioned strain rate gap. Characteristic stress–strain curves are shown in Fig. 12 for selected strain rates. In this figure, the maximum calculated strain does not exceed 1, according to the range of validity of Eq. (2). Such a strain corresponds to a vertical displacement of 0.7 mm. Yet, in the experiments, the maximum displacement reached a maximum value of 2 mm, corresponding to an extrapolated maximum equivalent strain of 2.85. This value is mentioned as an indication for comparison purposes only, until the range of applicability of Eq. (2) can be extended to higher strains.

As shown in Fig. 12, the strain rate sensitivity of OFHC copper is evident, but the nature of the flow curve is influenced by the strain rate as well. As the strain rate is increased, the strain hardening decreases, to reach an ideal plastic-like behavior at 0.6 s^{-1}. As the strain rate is increased the material exhibits negative strain hardening. By contrast, the stress–strain relation at high strain rates (Fig. 11)

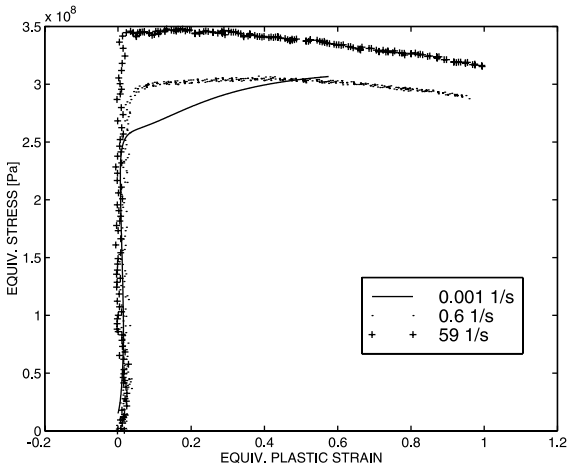

Fig. 12. Typical stress–strain curves for OFHC specimens deformed at nominal strain rates of 10^{-3}, 0.6 and 59 s^{-1}. Note the rate sensitivity of the material that affects both the flow stress and hardening characteristics.

exhibits little hardening and no softening in the investigated strain range. The reason for this discrepancy is not clear at that stage, and it appears that a detailed characterization of the microstractural changes in the gage material is required to characterize the mechanical behavior of this material. Preliminary results will be shown in the following section.

Fig. 13 displays the flow stress at an equivalent plastic strain of 0.5, as a function of the strain rate.

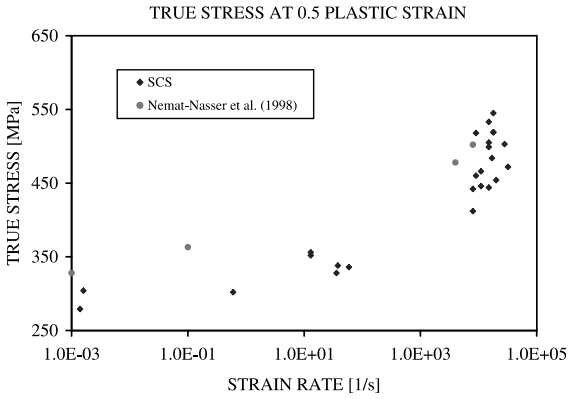

Fig. 13. Strain rate dependence of the flow stress of OFHC copper at an equivalent plastic strain of 0.5. The strain rate range varies from 10^{-3} to 3.2×10^4 s^{-1}. The results have been obtained using SCS only. Results by Nemat-Nasser et al. (1998) have been added for comparison purposes.

This figure illustrates the point that a wide range of strain rates can be investigated *with a single specimen type*. Results of Nemat-Nasser et al. (1998) have been added for comparison and illustration of the general good agreement between two different specimen geometries, namely the SCS and the CS.

3.5. Microstructural characterization

Microstructural characterization was performed by sectioning specimens at mid-thickness through the gage section. The specimens were polished and etched using standard metallographic techniques. The characterization included optical and scanning electron microscopy. Fig. 14 shows the general microstructure of the gage section and its vicinity in a specimen (#33) which was tested at a strain rate of $\dot{\varepsilon}_e = 18,000$ s^{-1}. The maximum equivalent strain was $\varepsilon_e = 2.2$, based on Eq. (2). The deformation of the gage appears to be homogeneous (Fig. 14a) and the reorientation of the grains inside the gage section is evident (Fig. 14b). Examination at a higher magnification reveals the presence of a boundary layer in which the flow of the grains is more pronounced. This narrow layer appears to be 50 μs wide and it is corroborated by the finite element calculation as well. An important point is that the deformation is confined and uniform over the gage section, so that the width of the deformed layer is not a variable. This point is further supported in Fig. 15, which shows the macroscopic cross section of another specimen (#43) which was deformed at a higher strain rate, $\dot{\varepsilon}_e = 28{,}000$ s^{-1}. Here, the maximum equivalent strain was $\varepsilon_e = 3.8$ (according to Eq. (2)). The gage section etches readily and is well delineated (Fig. 15a). Examination at higher magnification reveals a layer in which the individual grains are no longer discernable (Fig. 15b). The thickness of this layer is constant and equal to the gage thickness, thus revealing a uniform concentrated shear in the gage section. Similar but somehow less uniform layers has been observed in the top-hat specimens by Andrade et al. (1994), who also noted that the width of the shear layer increased with the strain.

Finally, microstructural examination of the deformed copper grains inside the sheared layer reveals a substructure of small equiaxed grains with

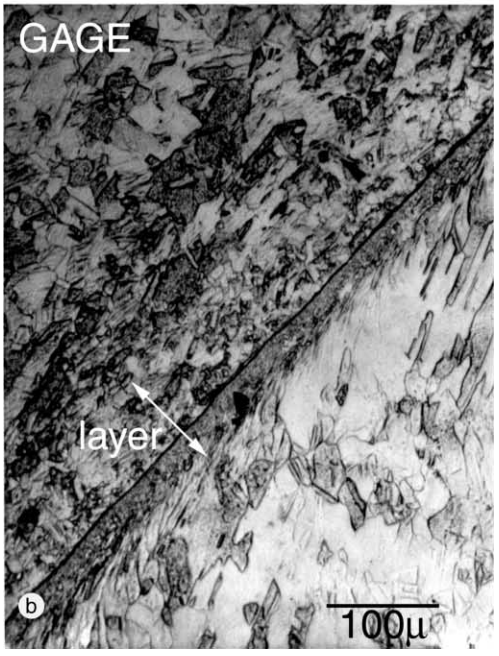

Fig. 14. Typical microstructure of the material used in the present study. Nominal strain rate of 18,000 s^{-1}, maximum strain of 2.2. The SCS has been sectioned perpendicular to the gage, and the depth of the section has been selected to outline the parallel lines of the gage section. (a) Low magnification. Note the uniform deformation of the gage material. Individual grains are discernable. (b) Higher magnification. Note the presence of a narrow boundary layer (about 50 μm) at the transition between the cylindrical part and gage section.

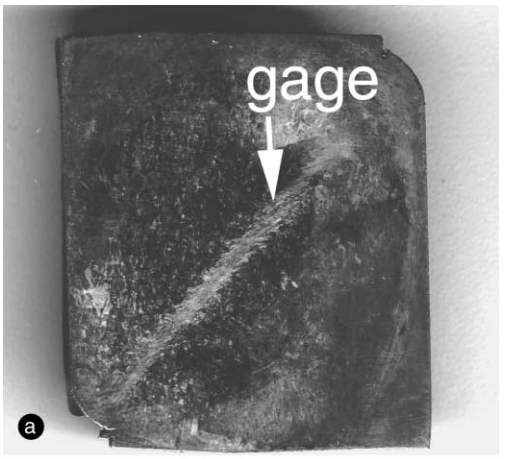

Fig. 15. Typical microstructure of the material used in the present study. Nominal strain rate of 28,000 s^{-1}, maximum strain of 3.8. The SCS has been sectioned perpendicular to the gage. (a) Low magnification. The gage section etches readily, showing a uniform deformation pattern. (b) Higher magnification. The individual grains in the gage are no longer discernable.

a typical average diameter of 1–2 μm (Fig. 16). Fine equiaxed grains have been identified as a result of dynamic recrystallization in this material by several authors (see, e.g. Andrade et al., 1994; Hines and Vecchio, 1997). However, the reports mention typical grain sizes of 150–300 nm for various

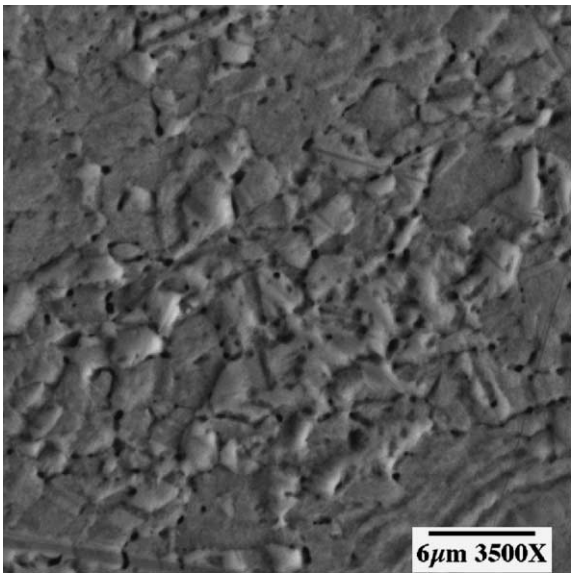

Fig. 16. Scanning electron micrograph, typical of the material inside the highly deformed grains of the specimen shown in Fig. 15. The high magnification reveals small, micron diameter, equiaxed grains which are characteristic of recrystallized material.

materials (e.g. Monel by Li et al., 2000), a size that is much smaller than the present observation, unless the deformation process was carried out at a higher temperature (523 K in Andrade et al., 1994). The kinetics of the recrystallization has not been addressed in the present study. A detailed study of the microstructure of the deformed material is currently under way and will be reported in the future. Hines and Vecchio (1997) reported that temperature rise associated with the thermomechanical coupling does not play a significant role in dynamic recrystallization. These authors calculated the temperature rise using a constitutive model Zerilli and Armstrong (1987). They found that the maximum temperature reached inside the sheared region was 500 K. At this stage, a simple estimate of the temperature rise can be obtained by assuming that all the mechanical work gets converted into heat in a supposedly adiabatic deformation process, according to

$$\Delta T = \frac{\beta W_p}{\rho C_p} \tag{4}$$

in which β, is the fraction of plastic work converted into heat (Mason et al., 1994; Kapoor and Nemat-Nasser, 1998; Rittel, 1999), W_p is the plastic work, ρ and C_p are the density and heat capacity respectively. For a representative stress level $\sigma = 500$ MPa (Fig. 11), $\varepsilon_{eq} = 3.8$, $\rho = 8890$ kg/m^3 and $c_p = 390$ J/kg K, equation Eq. (4) yields a temperature rise $\Delta T = 493$ K assuming $\beta = 0.9$. This result is quite consistent with the above-mentioned estimate. The final temperature is thus 0.56 times the melting temperature of copper ($T_m = 1356$ K).

4. Discussion

The results presented in this paper are centered on two main themes, namely the presentation and validation of a newly developed specimen for large strain and high-strain-rate characterization of metals, and its application to the characterization of OFHC copper.

The SCS has been studied in detail by numerical analysis, and that its main characteristics are the following. The gage section undergoes a shear dominant mode of deformation. The equivalent stress and strain are *uniform* over a *fixed length* corresponding to the height of the gage section. The numerical study has shown that the cylindrical parts of the SCS do not play a role other than load transfer through prescribed displacements to the gage section. As in the case of other commonly used specimens, simple relationships for the true stress and true strain have been proposed, on the basis of the numerical study. This was done once it was clear that the gage section does not undergo deformations corresponding to simple or pure shear. Therefore, the relationships involve *equivalent* measures of the stress and strain. Furthermore, these simple relationships do neither rely on assumptions of simple (pure) shear nor do they contain variable parameters such as the width of the shear layer.

Its simplicity makes the SCS attractive for constitutive testing over a wide range of strain rates (and temperatures). This was proposed, following the comparison of stress–strain characteristics obtained with the SCS and CS at various

strain rates. Consequently, the application of the SCS could be extended to higher strain rate characterization, both in the dynamic and in the "rapid" quasi-static domains. This resulted in the characterization of the constitutive behavior of OFHC copper over a wide range of strain rates, including two important domains of $\dot{\varepsilon}_e = 1$–100 s^{-1} and $\dot{\varepsilon}_e > 10^4$ s^{-1}. These domains are generally left unexplored due to limitations of the usual testing machines, or to specimen size requirements for the Kolsky apparatus. The important point is that the presented results were obtained using a unique *specimen geometry*. In this case, all the experiments carried out over a wide range of strain rates can be processed using similar equations, thus minimizing possible errors related to the uses of multiple specimen types.

As a remark, it should be noted that throughout this work, we have used Von Mises equivalent stress and strain values which do not take into account the development a deformation induced texture. Such a texture is responsible for the difference in the stress–strain curves obtained in tension, compression or torsion at large strains (Kocks et al., 1988). It appears that for OFE copper, there is a constant difference between the compression and torsion stress–strain curves. However, we have not attempted to take this effect into account, as this would require an additional study with a different emphasis.

Yet, there are two current limitations that require additional work. First is the uncertainty in the initial stress–strain curve part that relates to equilibrium considerations (due to the specimen finite dimensions). This limitation could be considerably reduced by additional numerical modeling of the gage section under dynamic loading, as the latter experiences equilibrium at the early stages of the deformation. In addition, slight geometrical changes, such as shortening of (one or both) the cylindrical sections of the SCS, would shorten the wave transit time through the specimen. The second limitation is related to the fact that deformations involving equivalent strains larger than unity have not yet been investigated. Here too, this limitation can be overcome by means of additional numerical work, using adequate techniques to account for the severe mesh distortion that are inherent to large deformations. The simple relationships given in Eqs. (2) and (3) can reasonably be expected to apply to higher strains.

The results obtained for OFHC copper are not new in the sense that this material has been extensively studied in the past. Yet, it is important to note that the present method yields results that are in agreement with the previous results. Nevertheless, beyond mere illustration purposes, specific points deserve additional attention. First, the metallographic examination has shown that the deformation of the gage is uniform, regardless of the equivalent strain. This observation is an additional validation of the numerical predictions. It is also interesting to note that the individual copper grains in the gage section remain discernable at fairly large strain levels ($\varepsilon_e = 2.2$, Fig. 14), to disappear at higher strain levels, for which recrystallized grains are observed, in the SEM ($\varepsilon_e = 3.8$, Fig. 15). While (dynamic) recrystallization was not the central point of this work, it is nevertheless felt that the proposed framework based on the SCS should yield additional interesting insight into the deformation mechanisms of structural materials at large strains, over a range of strain rates. Specifically, the difference in hardening behavior at the "rapid" quasi-static (1–100 s^{-1}) and high strain rates should be complemented by additional microstructural characterization using transmission electron microscopy.

5. Conclusions

- A new specimen (SCS), for large strain testing of materials, has been presented and analyzed.
- Numerical analysis of the SCS has shown that the state of strain and stress is quite complex and does not correspond to simple (or pure) shear, despite a dominant shear deformation. Yet, the equivalent plastic strain and stress are uniform over the gage section. Based on the numerical results, simple relationships were proposed to determine the equivalent plastic strain and stress.
- The numerical predictions were validated through comparisons with other specimen

geometries, existing results, and metallographic characterization of as received OFHC copper in the sheared gage section.
- The constitutive behavior of OFHC copper was investigated in the range of strain rates from 10^{-3}–10^{4} s^{-1} using a single specimen geometry.
- Traditional "gaps" in the achievable range of strain rates can be bridged using the SCS.
- The SCS offers a rigorous framework for the investigation of the constitutive behavior and deformation mechanisms of structural materials over a wide range of strain rates (and temperatures). SCS also provides a simple geometry for characterization of pressure sensitivity of dilatant materials such as polymers and porous materials and susceptibility of materials to shear banding.
- Additional work is required to extend the applicability of the stress–strain determination to equivalent strains larger than 1.

Acknowledgements

The research reported here was supported through a contract from the Sandia National Laboratories. G.R. acknowledges support from the Office of Naval Research (Drs. Y.D.S. Rajapakse and G. Yoder, Scientific Officers) for his research on Dynamic Behavior of Metals. We are pleased to acknowledge many helpful discussions with Dr. D. Dawson.

References

Andrade, U., Meyers, M.A., Vecchio, K.S., Chokshi, A.H., 1994. Dynamic recrystallization in high-strain, high-strain-rate plastic deformation of copper. Acta Metall. Mater. 42, 3183–3195.

Bodner, S.R., Rubin, M.B., 1994. Modeling of hardening at very high strain rates. J. Appl. Phys. 76, 2742–2747.

Clifton, R.J., 1990. High strain rate behavior of metals. Appl. Mech. Rev. 43, S9–S22.

Clifton, R.J., Klopp, R.W., 1986. In: Metals Handbook: Mechanical Testing, vol. 8. ASTM, Metals Park, OH.

Duffy, J., Campbell, J.D., Hawley, R.H., 1971. On the use of a torsional split Hopkinson bar to study rate effects in 1100-0 aluminum. J. Appl. Mech. 38, 83–91.

Hibbitt, Karlsson, Sorensen, Inc., 1996. ABAQUS/Standard User's Manual, Version 5.6.

Hines, J.A., Vecchio, K.S., 1997. Recrystallization kinetics within adiabatic shear bands. Acta Metall. Mater. 45, 635–649.

Kapoor, R., Nemat-Nasser, S., 1998. Determination of temperature rise during high strain rate deformation. Mech. Mater. 27, 1–12.

Klepaczko, J.R., 1998. Remarks on impact shearing. J. Mech. Phys. Solids 46, 2139–2153.

Kocks, U.F., Stout, M.G., Rollett, A.D., 1988. The influence of texture on strain hardening. In: Kettunen, P.O. et al. (Eds.), Strength of Metals and Alloys, ICSMA-8. Pergamon, NY, pp. 25–38.

Kolsky, H., 1949. An investigation of the mechanical properties of materials at very high rates of loading. Proc. Phys. Soc. London 62-B, 676–700.

Li, Q., Xy, Y.B., Lai, Z.H., Shen, L.T., Bai, Y.L., 2000. Dynamic recrystallization induced by plastic deformation at high rate in a Monel alloy. Mater. Sci. Engng. A 276, 250–256.

Mason, J.J., Rosakis, A.J., Ravichandran, G., 1994. On the strain and strain rate dependence of the fraction of plastic work converted into heat: an experimental study using high speed infrared detectors and the Kolsky bar. Mech. Mater. 17, 135–145.

Meyer, L.W., Manwaring, S., 1986. In: Murr, L.E. et al. (Eds.), Metallurgical Applications of Shock Wave and High-Strain Rate Phenomena. Marcel Dekker Inc., NY.

Meyers, M.A., 1994. Dynamic behavior of materials. John Wiley & Sons, NY.

Minnaar, K., Zhou, M., 1998. An analysis of the dynamic shear failure resistance of structural metals. J. Mech. Phys. Solids 46, 2155–2170.

Nemat-Nasser, S., Ni, L., Okinaka, T., 1998. A constitutive model for fee crystals with application to polycrystalline OFHC Copper. Mech. Mater. 30, 325–341.

Rittel, D., 1999. On the conversion of plastic work to heat during high strain rate deformation of glassy polymers. Mech. Mater. 31, 131–139.

Rittel, D., Lee, S., Ravichandran, G., 2000. A shear-compression specimen for large strain testing. Exper. Mech., in press.

Zerilli, F.J., Armstrong, R.W., 1987. Dislocation-mechanics-based constitutive relations for material dynamics calculations. J. Appl. Phys. 61, 1816–1825.